Scaling the Rock - A Micromechanical Model for the Elastic Properties of Hydrated Cement Pastes

by

Jonathan Bartholomew Estrada

Submitted to the Department of Materials Science and Engineering
in partial fulfillment of the requirements for the degree of

Bachelor of Science

at the

MASSACHUSETTS INSTITUTE OF TECHNOLOGY

June 2011

Author .....
Department of Materials Science and Engineering
May 6, 2011

Certified by .....
Krystyn J. Van Vliet
Associate Professor of Materials Science and Engineering
Thesis Supervisor

Accepted by .....
Lionel C. Kimerling
Professor of Materials Science and Engineering
Chairman, Undergraduate Thesis Committee

Scaling the Rock - A Micromechanical Model for the Elastic Properties of Hydrated Cement Pastes

by

Jonathan Bartholomew Estrada

Submitted to the Department of Materials Science and Engineering
on May 6, 2011, in partial fulfillment of the
requirements for the degree of
Bachelor of Science

Abstract

Cement is the most widely produced material worldwide. However, the understanding on how its nanoscale composition affect its microscale mechanical properties is limited. In this thesis, a micromechanical model for the purpose of cement hydration simulation was developed and tested using HYMOSTRUC3D hydration software and a micromechanical particle with interphase model developed by Deng and Van Vliet. It was then tested against empirical micro- and nanoindentation tests done on samples synthesized, cured, and prepared *in situ*. Preliminary mechanical calculations coupled with the hydration software show good agreement with experimental data. Additionally, predicted ranges of effective particle moduli values were found in nanoindentation testing. These observations support the validity of treating high density C-S-H as an interphase between low density C-S-H and clinker particles.

Thesis Supervisor: Krystyn J. Van Vliet
Title: Associate Professor of Materials Science and Engineering

Acknowledgments

I gratefully acknowledge funding and informative discussion of techniques and results provided by both CIMPOR and the Concrete Sustainability Hub.

I would like to thank many additional collaborators who provided extremely valuable insight, assistance, and contributions to the investigation. Thanks to Dr. Alan Schwartzman (DMSE) for training and advice on the Micromaterials Nanoindenter, and Angie Akono (CEE) and Muhannad Abuhaikal (CEE) for assistance with the CSM Microindenter/scratcher and polishing process, respectively. Additionally, many thanks are in order for Dr. J. Alberto Ortega (CEE) for assistance and guidance in Nanoindentation analysis techniques and Dr. Karen Stewart (formerly DMSE) for insight into cement synthesis and mechanical characterization techniques.

Furthermore, I would like to thank my thesis supervisor, Prof. Krystyn Van Vliet (DMSE) for her wisdom and expert advising on matters of cement, lab matters, and life itself. Additionally, thanks to Dr. Simone Musso (CEE), whose advice, assistance, and guidance on this project have been none short of exemplary, and Deepak Jagannathan (DMSE), who has worked with me closely in the experimental stages of the investigation. All three have been critically important to the work accomplished in this investigation.

Thank you to the members of both the CSHub and the Van Vliet Group. From Ilke's and Meng's help with the nanoindenter to Adam's sage advice, I am deeply grateful to have been part of such a high-caliber, collaborative research team. It has been an absolute pleasure working with each and every member and you all deserve the best in any and all of your future endeavors.

Finally, the utmost thanks are in order for my family - it is by their support and God's grace that I am studying at MIT, and without them I would not be half the researcher, student, or above all, person I am today.

Contents

List of Figures

List of Tables

Part I

Background Information

Chapter 1

Introduction

1.1 Project Background

Cement is the most widely produced material worldwide. In 2010 alone, an estimated 3.3 billion metric tons of cement were produced globally, with 63.5 million metric tons produced in the United States alone. Though the production of cement in the United States has declined in recent years, it has otherwise been steadily increasing around the world[17].

Cement is mixed with aggregate to form concrete. Due to its low cost, the abundance of its component materials, and its favorable compressive properties, it is used in many large-scale applications such as building foundations, structural components, bridges, dams, etc. However, there are considerable limiting factors in our current understanding of cement. One of the most prevalent questions stems from the largely multiscale nature of cement - how can we correlate cement's nanoscale properties with its microscale properties? Can our knowledge of the nano- and microscales be extended to better understand macroscale properties? The solutions to these questions could potentially provide answers to such large-scale issues as foundation cracking, CO_2 emissions through calcia reduction, and others.

1.2 Research Motivation

Cement is a particularly interesting and complex material - it has been used in some form since the Roman Empire developed a form of hydraulic cement around 20 AD [7], and yet historically has been an empirically understood material. Numerous additives have been used for the purpose of altering final mechanical properties, setting time, and freeze-thaw resistance to the resulting concrete. However, the different components and phases of cement are presently being modeled for the sake of detailed qualitative simulation and characterization. Additionally, the multiscale nature of cement presents a difficult problem - the link between the individual particles and phases and the composite properties is not readily obvious. This is due to dependence on hydration time, particle size, water to cement ratio, and a multitude of other parameters.

The aim of this investigation is to connect the nanomechanical mechanical properties of cement phases to the composite micromechanical properties via development and testing of a micromechanical model. The key to the investigation is generation of structural models and coupling results from the model with *in situ* nano- and micromechanical testing data for known cement compositions.

1.3 Experimental Objectives and Methodology

Experimental protocol consists of different techniques that aim to characterize cement pastes by both modeling and simulation techniques and mechanical testing. Using empirical nanoindentation grids and data sets along with microindentation tests provides valuable experimental insight to the accuracy of the developed model.

The scope of this investigation is defined by four objectives:

Objective 1: *Develop a micromechanical model to simulate hydration of cement pastes.* The investigation covered in this thesis primarily concerns the development of a micromechanical model, coupled with hydration simulations, to understand the connection between each phase's nanomechanical behavior and the composite mi-

cromechanical behavior.

Objective 2: *Develop the synthesis and preparation protocol for cement pastes with various additives.* The first step to understanding *in situ* cement pastes is to define the conditions by which they are synthesized. The cement sample synthesis, curing, and preparation methods are defined and detailed in this thesis. These methods must follow the American Society for Testing and Materials (ASTM) standards while suiting the needs of the investigation, and thus include additional cutting and polishing procedures necessary for mechanical testing.

Objective 3: *Discern the relevant mechanical properties of each cement paste using nanoindentation and microindentation tests.* Cement pastes exhibit different properties on different length scales– for microscale indentation tests, a composite modulus and hardness can be determined, while for nanoscale indentation tests, individual phases of cement, such as the local amorphous calcium-silica-hydrate gel phases, can be probed for the same mechanical information. In order to determine mechanical properties of each cement paste, instrumented indentation methods are utilized in this thesis.

Objective 4: *Correlation of experimentally verified properties with simulated properties.* After testing and data collection, the model is compared to the empirical data to determine the model's effectiveness. The parameter that is explicitly characterized and compared between the model and empirical data is the indentation modulus.

1.4 Outline of Thesis

This thesis is divided into four constituent Parts. Part I sets forth research goals and provides background information on cement chemistry, hydration, and other relevant topics for the investigation. The first Part continues to discuss the modeling aspect of the investigation, with relevant background information on previous models of cement hydration and discussion of micromechanics theory. It continues to set forth the model for cement hydration.

In the second Part of this thesis, the materials and methods for the experimental portion of the investigation are discussed and justified, with reference to ASTM standards and relevant theory and literature. Data analysis techniques for micro- and nanoindentation methods are also discussed in this Part.

In the third Part of this thesis, the mechanical results of the synthesized cement pastes are presented. This is followed by the fourth Part, which consists of a discussion of the results and analysis of the raw data. This Part then draws parallels between experimental observation and the proposed micromechanical model, finishing with conclusions and proposed options for future investigations.

Chapter 2

Background Information

2.1 Cement Chemistry

Before discussion of the mechanical properties of cement pastes, it is imperative to have an understanding of cement structure. Clinker, the unhydrated portion of cement, is composed of many different stoichiometric compounds. Additionally, there are many different kinds of cement, for a vast array of applications. The most common are called portland cement. Different types of portland cement are manufactured for different applications, but this investigation will use Type I, or Ordinary Portland Cement (OPC). Other variants exist as well, such as white portland cement (which lacks the typical grey color due to a reduction in ferrite)[6]. Each cement clinker is composed of various oxides which combine to form chemical phases. Common abbreviations for common oxides are shown in Table 2.1.

2.1.1 Pre-hydration Clinker

There are four principal constituent phases of cement clinker. The first two, C_3S, C_2S, are called alite and belite, respectively. The other two phases are tricalcium aluminate (C_3A) and tetracalcium aluminoferrite (C_4AF), more frequently called aluminate and ferrite. Alite is typically the dominant phase, representing 50-70% of cement clinker. Belite, C_3A, and C_4AF, make up 15-30%, 5-10%, and 5-15% of the clinker composi-

Table 2.1: Various abbreviations for the common simple compounds in cement. These abbreviations allow one, for example, to write C_3S instead of the more lengthy Ca_3SiO_5.

Chemical Formula	Abbreviation	Name
CaO	C	Calcium Oxide
SiO_2	S	Silicon Dioxide
Al_2O_3	A	Aluminum Oxide
Fe_2O_3	F	Iron(III) Oxide
MgO	M	Magnesium Oxide
H_2O	H	Water

tion, respectively. In addition to those mentioned, there are multiple other elemental oxides, making it clear that cement chemistry is quite complex. However, it is important to recognize that the chemistry of each clinker dictates many of the mechanical properties not just in the final, maximally-hydrated state, but as a function of time. For example, increasing the amount of alite in a given clinker increases the rate of hydration, but at a cost of ultimate strength. Additionally, alite is richer in calcium than the ultimately stronger phase of belite, which causes an environmental impact as well during the breakup of calcium carbonate into calcia and carbon dioxide. Thus, it is in our best interest to fully understand mechanical performance.

2.1.2 The Hydration of Clinker

Upon hydration of cement clinker, a multitude of compositionally varied phases arise. In addition to remnant anhydrous alite, belite, and metallic oxide compounds, new compounds form with water addition– these are SH_x, CH, and CSH. The ternary phase diagram of CaO, SiO_2, and H_2O is shown in Figure 2-1.

C-S-H and CH are extremely important with respect to the small-scale mechanical properties of hydrated cement. As the main products of hydration, they occupy roughly 50-60% and 20-35% of the hydration product volume, respectively[5]. C-S-H and CH result from the hydration of alite and belite, in the following proportions[1]:

[1]These reactions are approximate and are cited in different stoichiometries, such as in [5].

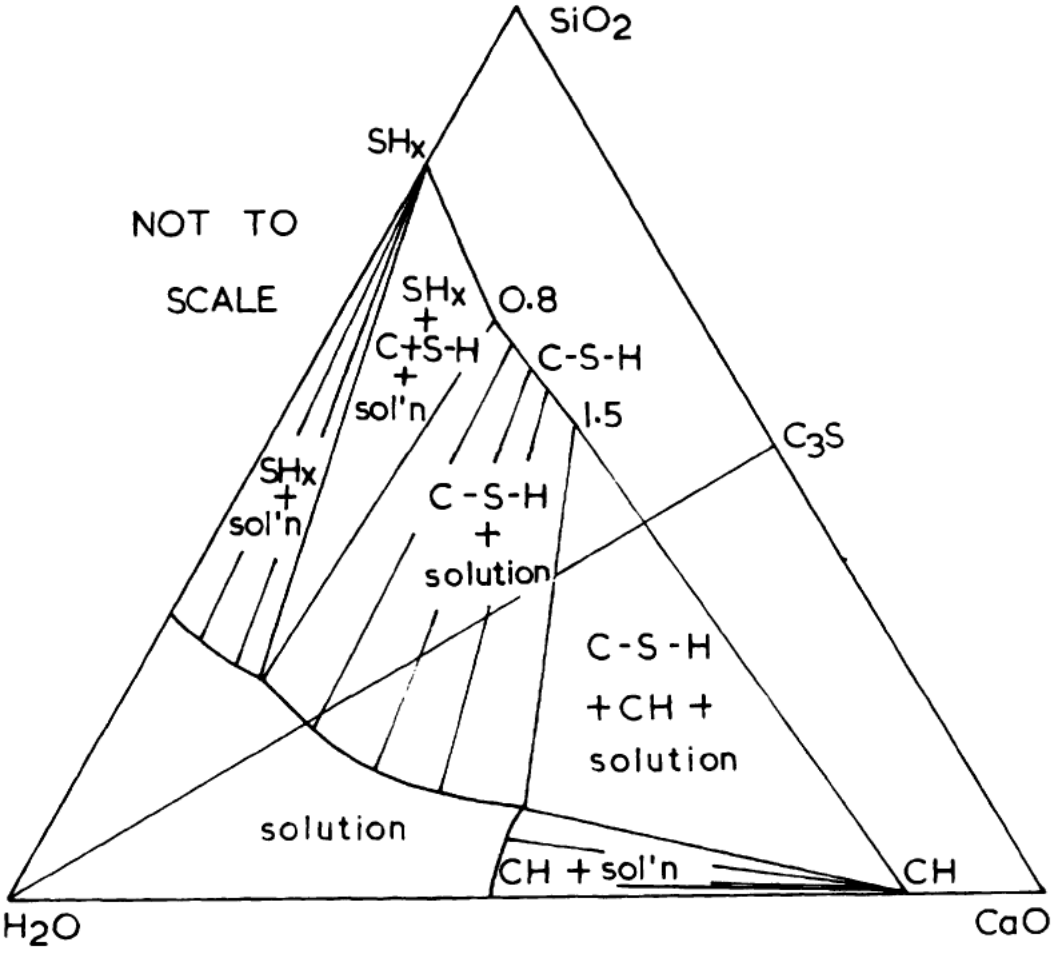

Figure 2-1: Ternary Phase Diagram of CaO, SiO_2, and H_2O. Note the stoichiometric variation in composition for C-S-H. Phase Diagram from [18].

$$2\ C_3S + 10.6\ H \longrightarrow C_{3.4}S_2H_8 + 2.6\ CH$$
$$2\ C_2S + 8.6\ H \longrightarrow C_{3.4}S_2H_8 + 0.6\ CH \tag{2.1}$$

It is important to note that C-S-H and CH are quite different. CH, known also as portlandite, is a crystalline phase with definite stoichiometry and well-known mechanical properties. On the contrary, C-S-H is amorphous and has different forms with different mechanical properties. These can be understood using the Jennings model of C-S-H formation shown in Figure 2-2.

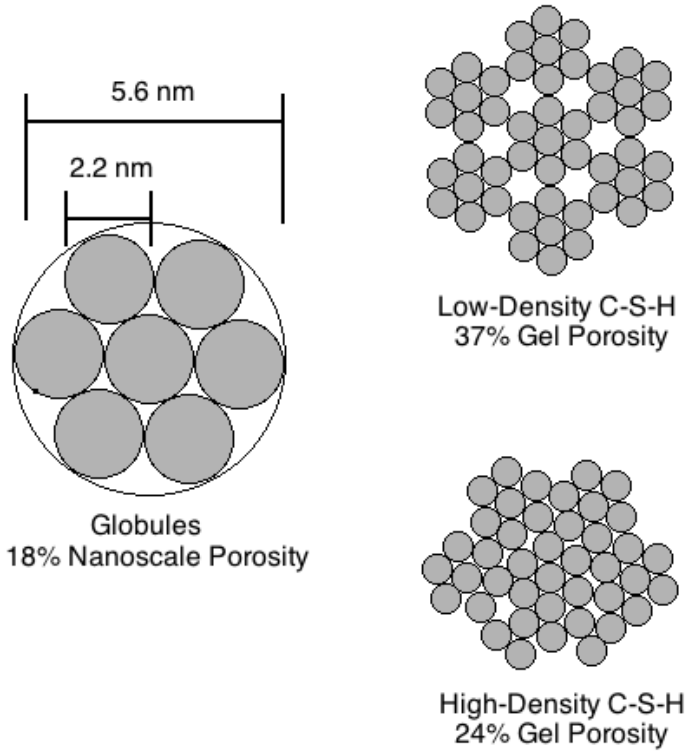

Figure 2-2: Jennings' colloid model for C-S-H types. C-S-H solid is formed by individual building blocks that pack in different ways, leading to two distinct phases - Low Density and High Density C-S-H, adapted from [8]

In Jennings' colloid model of C-S-H formation, each of the microscale hydration phases is created by 'globules', or clusters of the basic spheroidal building block of C-S-H. Inherent in each of these globules is 18 percent porosity, and the characteristic length is about 5.6 nanometers. The difference, therefore, between low density (LD) and high density (HD) C-S-H, stems from the packing of these globules. HD C-S-H packs very close to the close-packing density limit of hard spheres, at 76%. LD C-S-H packs closely to the randomly-packed density for hard spheres, at 63%. The characteristic dimension of LD and HD C-S-H is above 16.6 nm, but when the phases grow as hydration products on C_3S crystals, for example, the size becomes much larger, on the scale of 1-100 micrometers.

Using the Jennings model with hydration data from dried samples in [14], an empirical relation between the mass of LD C-S-H to the total mass of C-S-H in a

given paste was determined, and is given to be

$$\frac{m_{LD}}{m_{C-S-H}} = 3.017\frac{w}{c}\xi - 1.347\xi + 0.538, \tag{2.2}$$

where w/c is the water to cement ratio for the given sample and ξ is the degree of hydration, defined as the fractional mass of clinker that has reacted with water. Samples with lower water to cement ratios and/or large particle sizes will never reach full hydration.

2.2 Four-Level Thought Model of Cement

In a recent paper by Constantinidis [2], a thought model of cement hydration was developed in order to best explain the entire nanoscale to macroscale set of properties of cement. The first level (Level 0) is that of the single colloidal particle, as defined by Jennings. Level I is that of the C-S-H gel matrix, followed by Level II representing cement paste, and finally Level III representing mortar or concrete. Though this thesis sets out to model and verify the mechanical connection between Levels I and II, the overall perspective is certainly useful. Table 2.2 contains relevant properties of C-S-H and clinker phases for Levels I and II.

Table 2.2: Table of porosities and indentation moduli for the most common phases in cement gels and pastes. Adapted from [2].

Level/Phase	Density $[kg/m^3]$	Porosity [%]	Indentation Modulus $[GPa]$
I: LD C-S-H	1,930	37.3±0.1	18.2±4.2
I: HD C-S-H	2,130	23.7±0.1	29.1±4.0
II: CH (Portlandite)	2,240	-	38±5
II: C_3S (Alite)	3,150	-	135±7
II: C_2S (Belite)	3,280	-	130±20
II: C_3A	3,030	-	145±10
II: C_4AF	3,730	-	125±25

Chapter 3

Micromechanical Approach to Cement Pastes

3.1 Brief History of Micromechanics and Homogenization

One major stepping stone in the complete understanding of materials science is the connection between the properties we can see and measure on large scales and those we measure on significantly smaller scales. For simple materials (such as water, steel, rubber, etc.), modeling of the mechanical properties is relatively straightforward. Once we begin to look at heterogeneous media, however, the relative scale of inclusions or impurities plays a vitally important part in the mechanical properties of the entire material. For the general case of the stress strain response in a material, the stiffness tensor is fourth rank and appears as:

$$\underline{\sigma_{ij}} = \mathbf{C}_{ijkl}(x) : \underline{\epsilon_{kl}}. \tag{3.1}$$

This leaves a complex partial differential equation when used in motion or time-dependent situations. Hydration is a time-dependent process and therefore would require considerable work in order to be fully described. The question then persists: can we make assumptions to simplify the problem?

One convenient way to approach the problem is by homogenization. By this method, we can treat the solid as a one-phase matrix that exhibits a composite response, such as in Figure 3-1. This scenario is applicable when there are few interactions between inclusions.

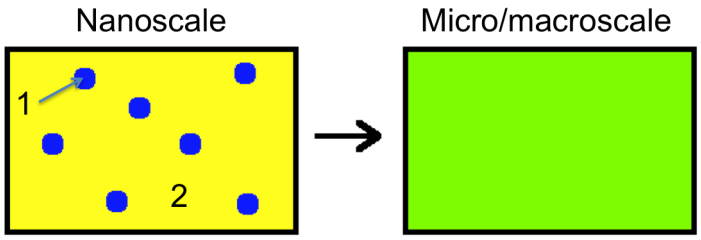

Figure 3-1: The basic concept behind the model of homogenization.

3.1.1 Eshelby's Tensor

By treating the inclusion in a matrix as its own entity, allowing it to take the eigenstrain of the system, and then applying strains to the inclusion to fit it back into the matrix, J.D. Eshelby revolutionized the field of mechanics of materials. The Eshelby tensor for the general case in dilute concentrations is defined as [13]:

$$\mathbf{C}_*^d = \mathbf{C}_0 + \phi(\mathbf{C}_1 - \mathbf{C}_0)\mathbf{A}, \tag{3.2}$$

where $\underline{\epsilon_i} = \mathbf{A} : \underline{\epsilon_f}$, or the inclusion strain tensor ϵ_i is related to the far-field strain ϵ_f by the fourth rank Eshelby tensor, $\mathbf{A}$. When applying Eshelby's tensor to particular applications, $\mathbf{A}$ includes parameters that relate shape to the effective bulk and shear moduli of each inclusion. However, as Eshelby noted himself [4], solving for the external field is quite difficult for cases that are not simple. Luckily, a spherical approximation is suitable for this investigation of cement hydration.

3.1.2 Bar Model

When inclusions can be simplified to regular shapes and occur in periodic, but low frequencies, the classical asymptotic homogenization method can be used, such as in [15]. By taking a linear section of the material, we can model the effective elasticity response of the material as Hookean, e.g.

$$E_{bar} = \frac{E_m E_i}{(1 - f_i)E_m + f_i E_i}, \tag{3.3}$$

where the subscripts m and i denote the matrix and inclusion, respectively, and f_i is the volume fraction of the inclusion. This is very useful for well-dispersed solids and can be used in the current case of cement hydration to help describe clinker inclusions in a matrix of low density C-S-H. However, an issue remains - the HD C-S-H phase forms an interphase between clinker and LD C-S-H, which must be taken into account on such small scales, making additional complexity necessary for a reasonable cement hydration model.

3.2 Model of Composites with an Interphase

Upon hydration at low water-to-cement ratios, two distinct phases of C-S-H form - low density and high density C-S-H. This has been modeled by Constanidis and Ulm [2] as shown in Figure 3-2.

Deng and Van Vliet [3] developed a model which, in its most general case, takes both the relative number of inclusion particles and the mechanical properties of a region between the inclusion and matrix phases. This interphase region, when the particles are very small, can be very influential on the resulting mechanical properties of the system. Thus, the Deng-Van Vliet model defines an "effective particle", which is relevant to the cement model. The bulk and shear moduli, K and G, are defined for the effective particles as follows:

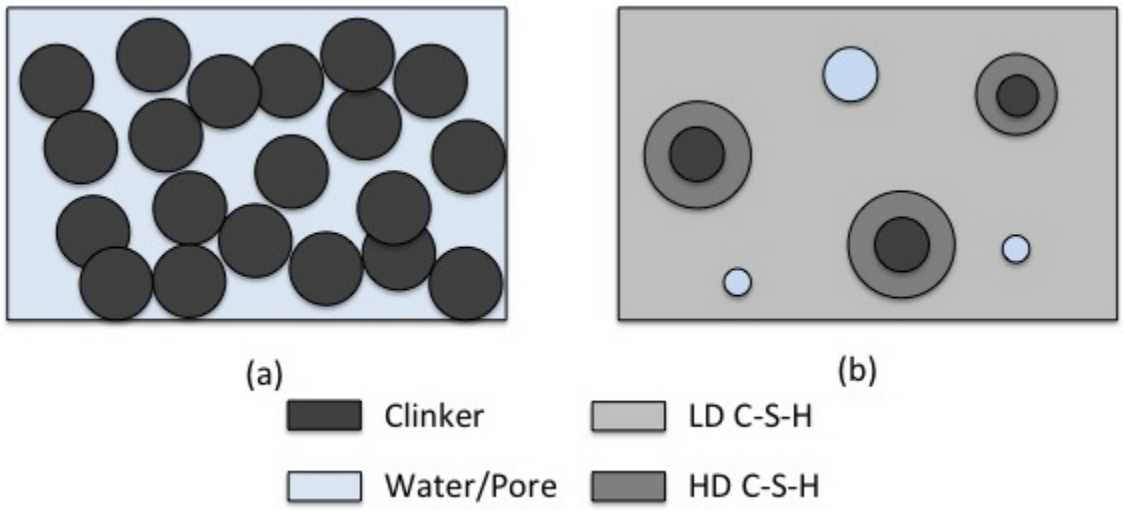

Figure 3-2: Schematic of the hydration of cement, adapted from [2]. (a) shows the first stage of the clinker-water reaction, where C-S-H nucleates from clinker particles. (b) shows the later stages, where HD C-S-H has nucleated around clinker particles in an overall matrix of LD C-S-H.

$$K_{EP} = K_I \left(1 + \frac{(K_I/K_P - 1)a}{1 + \eta_I(1-a)(1-2\nu_I)(K_I/K_P - 1)}\right)^{-1} \tag{3.4}$$

$$G_{EP} = G_I \left(1 + \frac{(G_I/G_P - 1)a}{1 + \delta_I(1-a)(1+\nu_I)(G_I/G_P - 1)}\right)^{-1} \tag{3.5}$$

where I and P represent the interphase and particle inclusion, respectively and a is the volumetric ratio of the original inclusion to the inclusion plus the shell. The two parameters η_I and δ_I stem from the Eshelby tensor, and can be written for the case of a spherical particle as:

$$\eta_I = \frac{2}{3\,(1-\nu_I)}$$

$$\delta_I = \frac{7 - 5\nu_I}{15\,(1-\nu_I^2)} \tag{3.6}$$

Substituting in parameters relevant to the cement hydration model into equations 3.4 and 3.5 give the following relationship:

$$K_{EP} = K_h \left(1 + \frac{(K_h/K_c - 1)\left(\frac{r}{r+t}\right)^3}{1 + \eta_I(1 - \left(\frac{r}{r+t}\right)^3)(1 - 2\nu_h)(K_h/K_c - 1)} \right)^{-1} \tag{3.7}$$

$$G_{EP} = G_h \left(1 + \frac{(G_h/G_c - 1)\left(\frac{r}{r+t}\right)^3}{1 + \delta_h(1 - \left(\frac{r}{r+t}\right)^3)(1 + \nu_h)(G_h/G_c - 1)} \right)^{-1} \tag{3.8}$$

where the subscripts c represents clinker and h represents HD C-S-H. The variable r refers to the radius of the clinker particle and t represents the thickness of the interphase, or HD C-S-H shell. For the entire nanocomposite behavior according to [3], the relation in this scenario is given as

$$K = K_l \left(1 + \frac{(K_l/K_{EP} - 1) f_{EP}}{1 + \eta_I(1 - f_{EP})(1 - 2\nu_l)(K_l/K_{EP} - 1)} \right)^{-1} \tag{3.9}$$

$$G = G_l \left(1 + \frac{(G_l/G_{EP} - 1) f_{EP}}{1 + \delta_I(1 - f_{EP})(1 + \nu_l)(G_l/G_{EP} - 1)} \right)^{-1} \tag{3.10}$$

where the subscript l refers to the LD C-S-H matrix phase and f_{EP} is the volume fraction of effective particles. In [3], a second model for agglomeration of particles is proposed as well, for when the fraction of particles is high enough for interaction between effective particles. Though this does not demand percolation, it still results in a composite structure that contains regions of both matrix surrounded by aggregated particles and vice versa.

In cement hydration, there is an interesting coupling of mechanically different phases– during hydration, the clinker particles, originally of some size r_0, decrease in size at the expense of C-S-H growth. Due to this shrinkage of the volume of clinker, it is a reasonable assumption to say that effective particles (which comprise solely of

clinker and HD C-S-H) are, in fact, distinct from one another. Thus, the equations 3.7-3.10 suffice to describe the system mechanically.

3.3 Usage of HYMOSTRUC to Generate 3D Structures

The model described by equations 3.7-3.10 is informative and offers insight as to the composite response of cement pastes, but the conditions upon which it is valid are necessarily limited to high degrees of hydration ($\xi > 0.5$). Thus, for simulation and understanding of the entire time-dependent process of hydration of cement pastes, more complicated methods are necessary. There are multiple computer simualtion programs (as reported by [19]) that are capable of simulating cement pastes, such as Jennings and Johnson's early simulation model [9], the National Institute of Standards and Technology (NIST) CEMHYD3D model, the HydratiCA developed by Bullard at NIST, and Bishnoi and Scrivener's μic model for hydration [1].

However, for some simplification of the problem and usage of spherical inclusions, the HYMOSTRUC3D software, developed at the Delft University of Technology in the Netherlands, was selected for usage. HYMOSTRUC offers a wide array of useful options that allow for case-studies and provides visual output for hydration step times. Additionally, options for water to cement ratio, clinker composition, air inclusions, hydration temperature, and particle size are all fully customizable. Using standard particle size distributions and declaring the aforementioned variables, a hydration model can be constructed. An example of the initial clinker placement and hydration is shown in Figure 3-3.

By coupling the generated statistical HYMOSTRUC models and the Deng-Van Vliet micromechanical model for particles with an interphase, we can get a resulting composite modulus, which should be measurable at scales much larger than the relevant size of the small clinker particles.

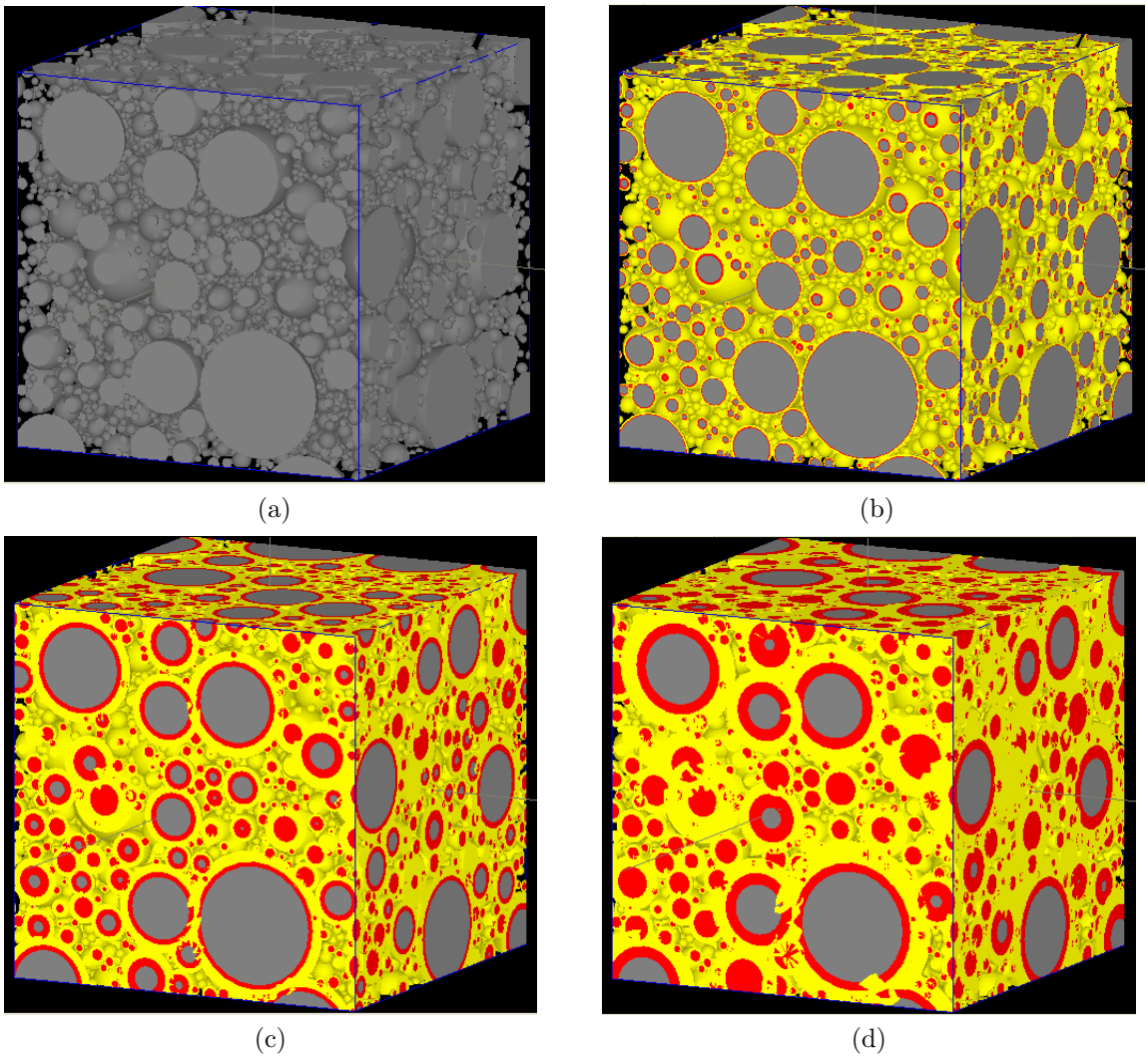

Figure 3-3: HYMOSTRUC3D cement hydration simulation of a volume of 100 μm on a side, at (a) $t = 0$, (b) $t = 10$ hrs, (c) $t = 100$ hrs, and (d) $t = 1000$ hrs. The grey areas represent clinker, the yellow areas represent LD C-S-H nucleation, and the red areas represent consumed clinker.

Part II

Experimental Materials and Methods

Chapter 4

Instrumented Indentation Theory

4.1 Introduction

Cement, as has been discussed previously, is a porous materlal. It contains porosity on the nanoscale (in LD and HD C-S-H), on the microscale (C-S-H pores that form during hydration), and on the macroscale (trapped air bubbles from mixing, etc.). Different scales of instrumented indentation can be used to find elasticity and hardness measurements. Though for fully homogeneous systems, these properties should remain the same on, for example, nano- and microscales, this is not the case for cement. Cement is clearly heterogeneous, with characteristic phases on many different scales. However, information from the nanoscale can potentially be linked to that of the microscale via a composite model; this is the reason for experimental verification. In this investigation, both micro- and nanoindentation are used for mechanical testing.

4.2 Instrumented Indentation Theory

The basic principle of an indentation test is the following: an input load P is applied to a material and the response is an output displacement, h. This is done continuously over some period of time, and by varying P and monitoring h simultaneously, intrinsic material properties can be measured. The most common usage of indentation data

is to obtain values for indentation modulus M and indentation hardness H, though other values, such as plastic work, elastic work, and contact compliance, can be used for mechanical characterization. In this investigation, M and H are the most relevant mechanical properties and thus will hold the primary focus.

Pyramidal indenter probes are commonly used as they can test volumes of materials smaller then their counterparts. The most commonly used pyramidal indenter probe, which has been shown to yield characteristic indentation curves for cement in [20], is the Berkovich probe. The Berkovich probe shares the same equivalent half angle, $\theta = 70.32°$, as the Vickers probe historically used for hardness testing. The geometry for an indenter test is shown in Figure 4-1.

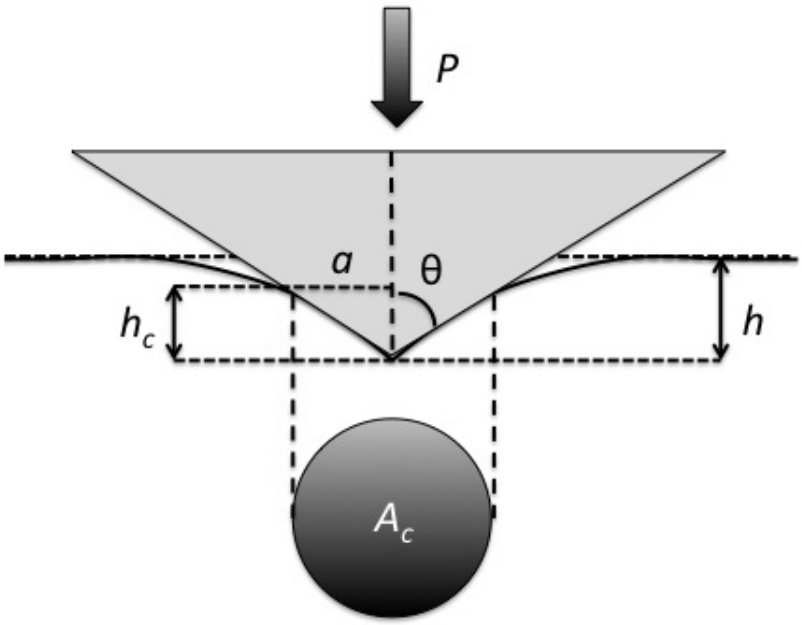

Figure 4-1: Geometry of an individual indentation test, as adapted from [20]. As a load P is applied to a material, a height h is registered. The area A_c represents the projected contact area, determined by the angle θ, contact depth h_c, and contact radius a.

As shown in [20], the self-similarity of the indentation test due to the geometry of the Berkovich indenter and the ratio of contact height to indentation depth are independent of the applied load P. This independence allows the hardness, H, to remain a material property independent of P and gives it a degree of statistical robustness.

4.2.1 Oliver and Pharr Method

One of the more common ways of analyzing nanoindentation data is by using the Oliver and Pharr method[12], which develops both hardness and indentation modulus for a given indentation curve. Due to self-similarity of the indenter probe and height to indentation depth being independent of the load, as previously mentioned, the hardness can be written as:

$$H = \frac{P_{max}}{A_c} \tag{4.1}$$

The indentation modulus, M, is defined with respect to the unloading curve of the material[10]:

$$\frac{dP}{dh} = \frac{2}{\sqrt{\pi}} M \sqrt{A_c}, \tag{4.2}$$

where dP/dh is also known as the contact stiffness, S. The indentation modulus, also known as the reduced modulus, is actually a function of two different materials, as both the tested material and the indenter itself have an effect on the measured modulus. The relation is given as:

$$M = \left[\frac{1-\nu^2}{E} + \frac{1-\nu_i^2}{E_i} \right]^{-1}, \tag{4.3}$$

where the first set of elastic properties pertain to the material and the second set, denoted with subscript i, are properties of the indenter. The latter are constant through all measurements, and thus the material properties can be probed.

4.2.2 Indentation Length Scales

For measurements to have any meaning, they must obey the assumption of homogeneity on the scales which are to be measured. For a representative elementary volume of the material with characteristic dimension, L, individual test spacing distance, x, and largest heterogeneity size, d, the scale separability condition must be obeyed (as per [2]):

$$d \ll L \ll x. \tag{4.4}$$

This simply means that for an assumption that the material is made up of elementary volume elements, the heterogeneities should be such that uniform properties can be assumed. For the cement samples tested in this thesis, the analysis is done under this assumption, and from those measurements a packing density can be determined of the local C-S-H phase. Before any of this can be determined, however, it is imperative that the microstructure is not too large for these measurements - otherwise, the usage of classical continuum mechanics is not appropriate.

4.2.3 Grid Indentation

The principle underlying grid instrumented indentation is the relative scale difference between heterogeneous features, which is well summarized in Figure 4-2. For nanoindentation, the characteristic phase sizes (i.e. LD and HD C-S-H phases nucleating from clinker particles) are on the order of 10 μm and up, while indentation depth is generally only 200-300 nm. The spacing between tests is set even larger (in this thesis, 20 μm) to ensure isolated mechanical measurements.

Mathematically, grid indentation with a large sample size allows a reasonable approximation to the phase distribution of the heterogeneous cement paste. It is by this method that the fraction of LD and HD C-S-H can ideally be approximated. Assuming normal distribution of the particles in the measurement area and a large number of indentations, the case of cement paste indentation can be approximated as follows:

$$\phi_i = \frac{1}{V} \int_V \delta_i d\underline{x} \approx \frac{1}{n} \sum_{j=1}^{n} \delta_i, \tag{4.5}$$

where i corresponds to a certain phase in the material, ϕ is the volume fraction, V is a characteristic volume of the material, δ is the Dirac delta function, and n is the total number of indentations.

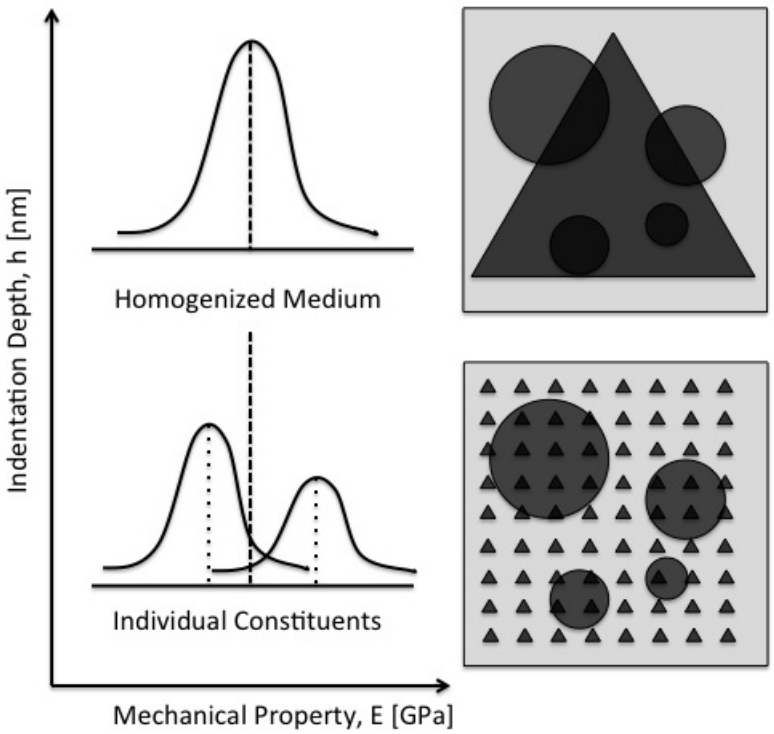

Figure 4-2: Schematic, adapted from [2], showing the principle underlying grid-nanoindentation for heterogeneous cement pastes. For shallow depths, individual phases can be probed for mechanical information. For very deep indentations, however (such as in the case for microindentation), the measured property is that of a homogenized material.

The chief purpose of instrumented indentation used in this setting is to use two different length scales of measurement to determine both the individual phase and composite phase mechanical response of cement pastes. Nanoindentation results yield measurements that pertain to an individual phase's mechanical properties. Though this would appear to be straightforward, other variables, such as porosity, are of considerable importance in these measurements. Microindentation, on the other hand, yields a composite response for the modulus and hardness values. Thus, by coupling this experimental data with the micromechanical model discussed in Chapter 3, a connection can be determined by simulation and subsequently verified.

Chapter 5

Materials and Methods

5.1 Cement Synthesis

For this investigation, a cement synthesis protocol was developed in accordance with ASTM standards. The procedure is as follows:

1. **Choice of Composition** Sixteen (16) different samples were created according to a Taguchi-method[1] matrix. Five parameters were altered (staying consistent with a L16' matrix. Each parameter contained a total of up to four different factors, or variations, of that parameter. The parameters and associated factors are shown in Table 5.1.

2. **Synthesis Technique** - For each set of samples, 40 g of cement clinker was mixed with the necessary amount of water (as given by the water to cement ratio). Fly ash, if applicable, was added as 30 $wt\%$ of the solid constituent, without any change of the water to cement ratio. For the samples mixed with initial pH = 4, a solution of pH = 4 aqueous HCl was prepared. The constituents were mixed by first adding the water or aqueous HCl to a 50 mL Falcon centrifuge tube, followed by fly ash if applicable, and then quickly followed by all of the cement clinker. A few hand-mixing revolutions with a spatula were then

[1]Though this thesis does not cover Taguchi theory, it should be known that this investigation overlapped with a concurrent study on the chemomechanical comparison of various cement pastes by S. Musso, J. Estrada, D. Jagannathan, F.-J. Ulm, K. Van Vliet, et al.

Table 5.1: Various additives contained in samples 1-16, arranged into their respective categories. Each parameter shown across the top has four associated factors, which are subsequently combined into the Taguchi matrix to get the maximum number of different combinations.

Factor	**Temp.** $(^{\circ}C)$	**W/C Ratio**	**Fly Ash**	**Clinker Type**	**pH**
1	60	0.43	None	Pure C_3S	7
2	40	0.40	None	White Cement	7
3	20	0.37	Class F High-activated C	OPC	4
4	5	0.34	Class F Low-activated C	Pure C_2S	4

succeeded by capping the tube and using a VWR Vortexer at speed 8. After 2 minutes and 30 seconds, the tube was opened and a spatula was used to ensure that clumps did not form. Once this was ensured, the tube was recapped and placed upside down on the vortexer, allowing the mix from the bottom to become the new top surface, for 30 seconds. The tube was then placed right side up on the vortexer, mixed for another 30 seconds, and this is repeated until $t = 5$ minutes. The tube containing the mix was then emptied, with the aid of the spatula, into three 25mL polystyrene (PS) petri dishes. The three samples were then mechanically agitated via tamping to remove macroscopic air bubbles.

3. **Initial Storage and Demolding** - Each of the three samples was initially stored in the mold for a day, or upon being solid enough to remove from the mold. The petri dishes were placed in the respective temperature environment in a high-humidity environment, ensured by a closed container partially filled with deionized water. Once the sample was hard enough to be removed from the PS dishes, a Dremel tool was used to carefully cut the PS dish away from the sample.

4. **Curing Procedure** - After mold removal, the three samples were placed in a numbered jar containing a saturated solution of $Ca(OH)_2$ for curing, and placed back into the respective location with associated temperature value. Curing

lasts for 28 days.

5. **Hydration Halting** - After curing for 28 days, samples were removed and fully submerged in a different jar containing a mixture of 6 parts methanol, 7 parts isopropyl alcohol, and 2 parts anhydrous ethanol, for one week. After this, the samples are put in a vacuum chamber for a day and subsequently vacuum sealed in plastic bags using a Food Saver®.

5.2 Polishing Technique

In order to polish different cuts from the sample discs made in the aforementioned synthesis procedure, a Buehler IsoMet diamond saw was used. Thin slices were made perpendicular to the round faces of each sample at a thickness of approximately 5 mm. These then had to be cut such that they fit on atomic force microscope (AFM) discs, 1 cm in diameter. The small cuts of cement were then individually mounted on the AFM discs using a very thin coating of super glue.

Each of the cut and mounted cement samples was then placed upside-down in a custom-made jig which served to apply pressure to the sample during polishing while securing the sample completely. The process occurred on a rotating wheel with a Buehler TexMet-P polishing pad. The polishing pad consists of a hard, perforated surface on which colloidal suspensions can be sprayed and excess material can be polished and removed from the system. Nine micron colloidal silica solution was sprayed on the pad and the samples were polished for anywhere from 10 minutes to a few hours, depending on initial quality of the sample from the diamond saw cutting process. The initial polishing procedure is shown in Figure 5-1.

After the initial polishing process, the samples were moved to a separate location where they were cleaned by submerging in *n*-decane and ultrasonic cleaning. After air-jetting the remaining *n*-decane from the surface, the samples were hand-polished by rubbing the samples on pads of four different grain sizes in order from largest particle size to smallest: 9μm, 3μm, 1μm, 0.3μm, respectively. The sample was polished on the first, air-jetted, and then polished on the next pad, continuing until the smallest

Figure 5-1: [Top] Sample mounted on AFM disc. [Bottom] Polishing instrumentation with jig and holder.

grain size. Finally, the sample is again put through ultrasonic treatment, air-jetted, and stored promptly in the Food Saver® bags. When any sample was subsequently used, it was cleaned with isopropyl alcohol immediately before use in order to get rid of surface impurities.

5.3 Instrumented Indentation

5.3.1 Nanoindentation

Nanoindentation was performed on a MicroMaterials NanoTest NTX Nanoindenter, shown in Figure 5-2. Due to the high heterogeneity of cement paste, it is advantageous

to perform as many tests as possible to determine the distribution and properties of the constituent phases most accurately. Previous experiments (such as Miller et al. [11] and Stewart, Shahsavari, et al. [16] have used 300-400 point nanoindentation grids to varying degrees of repeatability. In this investigation, 1000 points were taken per sample in order to ensure repeatability and overcome some of the effects of macroporosity.

A Berkovich probe was used with the following loading parameters: loading rate = 12 mN/min, dwell period = 5 s, unloading rate 12 mN/min. The peak load was defined to be 2 mN. Two square grids of 400 (20 x 20) and one rectangular grid of 200 (20 x 10) indentation tests were performed, with spacing between adjacent points set to 20 μm. Individual indentation maps of indentation modulus and hardness as a function of position were developed using a self-created MATLAB script. Indentation modulus and hardness were both calculated using the Oliver-Pharr method for each individual indent.

5.3.2 Microindentation

Microindentation was performed on a CSM Instruments Micro-Combi Tester. The principle behind the microindenter is essentially the same as the nanoindenter, though with a much larger Berkovich tip. The loading rate and unloading rate were both set to 10 N/min, with a dwell period time of 10.0 s and maximum load of 10 N. Due to the expected composite response, only 5-9 indentation points for each sample were tested (as opposed to the 1000 points for each nanoindentation test). Indentation modulus and hardness were again both calculated from load-displacement curves using the Oliver-Pharr method.

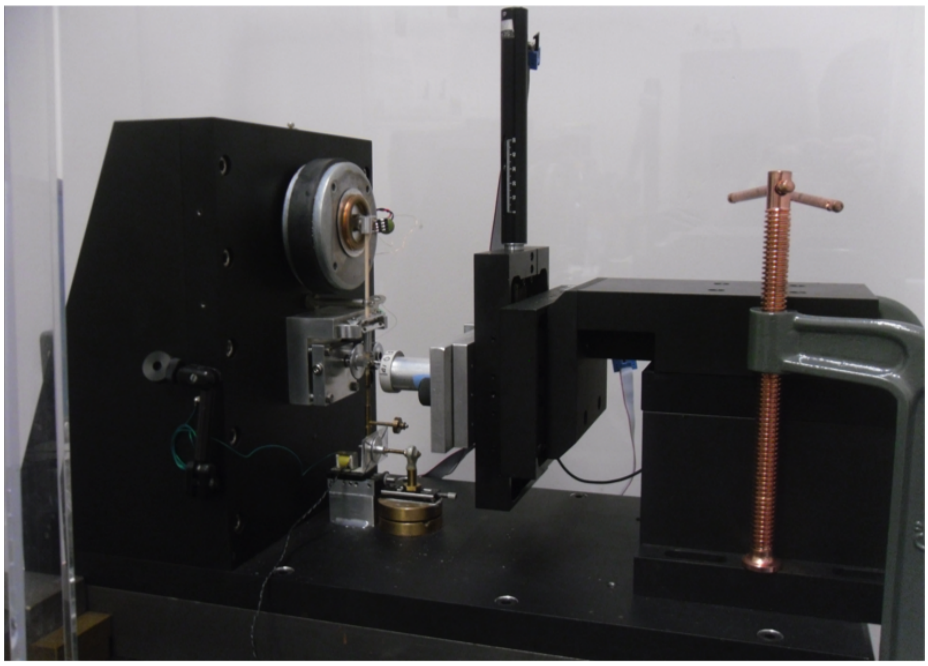

(a)

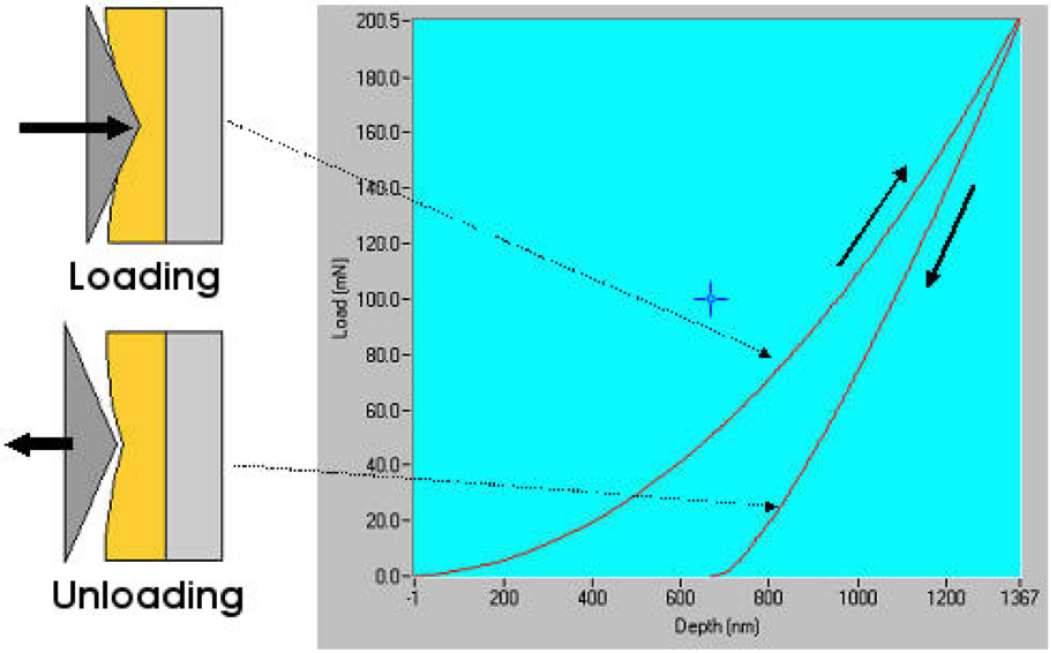

(b)

Figure 5-2: (a) Picture of the Micro Systems Ltd. nano-k indenter loaded with a cement paste sample. (b) A loading/unloading hysteresis curve that is typical of nanoindentation. The indenter tip contacts the surface and lowers until a desired load is reached, finally unloading and releasing from the plastically deformed material.

Part III

Results

Chapter 6

Micromechanical Modeling

6.1 Input Parameters

As discussed in Chapter 3, the intention of this investigation is to take the mechanical properties of two different types of C-S-H on the nanoscale and correlate them to micromechanical composite properties using a cement hydration model. Therefore, we must use a model that takes into account the various input parameters which comprise the cement samples.

HYMOSTRUC was used to simulate 6 of the total samples[1]. The compositions of each of these samples is tabulated in Table 6.1. The first step to simulation of

Table 6.1: Properties and names of the six modeled and experimentally measured samples.

Sample No.	**Name**	**Temp.** $(^{\circ}C)$	**W/C Ratio**	**Clinker Type**	**pH**
1	A7N60	60	0.43	Pure C_3S	7
2	W7N60	60	0.40	White Cement	7
5	G4N20	20	0.43	OPC	4
11	W4N40	40	0.37	White Cement	4
12	A4N40	40	0.34	Pure C_3S	4
16	G7N05	5	0.34	OPC	7

[1]This was due to that (a) fly ash could not be included in the software and (b) the C_2S samples were not mechanically viable for instrumented indenter testing.

the 6 samples was to define the initial conditions chemically to coincide with the experimental method. This included the cement constituent oxide composition, the water to cement ratio, particle distribution size, and hydration rate. The constituent oxide ratio for OPC was provided by the software, while that for white cement was given by [6]. The particle distribution size is given by the Weibull distribution function (also known as the Rosin-Rammler distribution),

$$f(x;k,\lambda) = \frac{k}{\lambda}\left(\frac{x}{\lambda}\right)^{k-1} e^{-(x/\lambda)^k}, x \geq 0, \tag{6.1}$$

where k and λ are the particle size spread and mean particle size, respectively. These are automatically defined in HYMOSTRUC via the Blaine parameter, a measure of surface area per kg of cement. The specifications for composition, Blaine number, and particle size, though not explicitly known for the experimental OPC and white cement, are presumed to be similar to those tabulated in [6], and are reproduced in Table 6.2.

Table 6.2: Chemical and compound composition and Blaine fineness of pure alite, type II ordinary Portland cement, and white cement.

Cement	Chemical Composition, %						Compound Composition, %				Blaine no.
Type	SiO_2	Al_2O_3	Fe_2O_3	CaO	MgO	SO_3	C_3S	C_2S	C_3A	C_4AF	$[m^2/kg]$
OPC[2]	20.9	5.2	2.3	64.4	2.8	2.9	55	19	10	7	370
White	24.5	5.9	0.6	65.0	1.1	1.8	32	50	15	2	490
C_3S	26.3	0.0	73.7	0.0	0.0	0.0	99.9	<0.1	0	0	625

Once the parameters were set, the hydration duration was set to the same length as the empirically measured samples, or approximately 28 days.

6.2 HYMOSTRUC3D Output Data

After setting up the initial conditions, HYMOSTRUC fills the model cell with the Weibull distribution of particles, proceeding to then hydrate each size of particle at a varying volumetric rate which increases as the ratio of surface area to volume drops.

As the timestep progresses, the particles become more and more hydrated, eventually impinging on each other to form a matrix of clinker, C-S-H, and pores.

HYMOSTRUC outputs different valuable parameters that are useful in determining information about the mechanical properties of the resultant paste - these include the number of particles, the individual clinker particle hydration, and the resulting growth radius of C-S-H, all as a function of initial radius. Graphs of hydration versus initial clinker radius for the 6 different samples are shown in Figure 6-1.

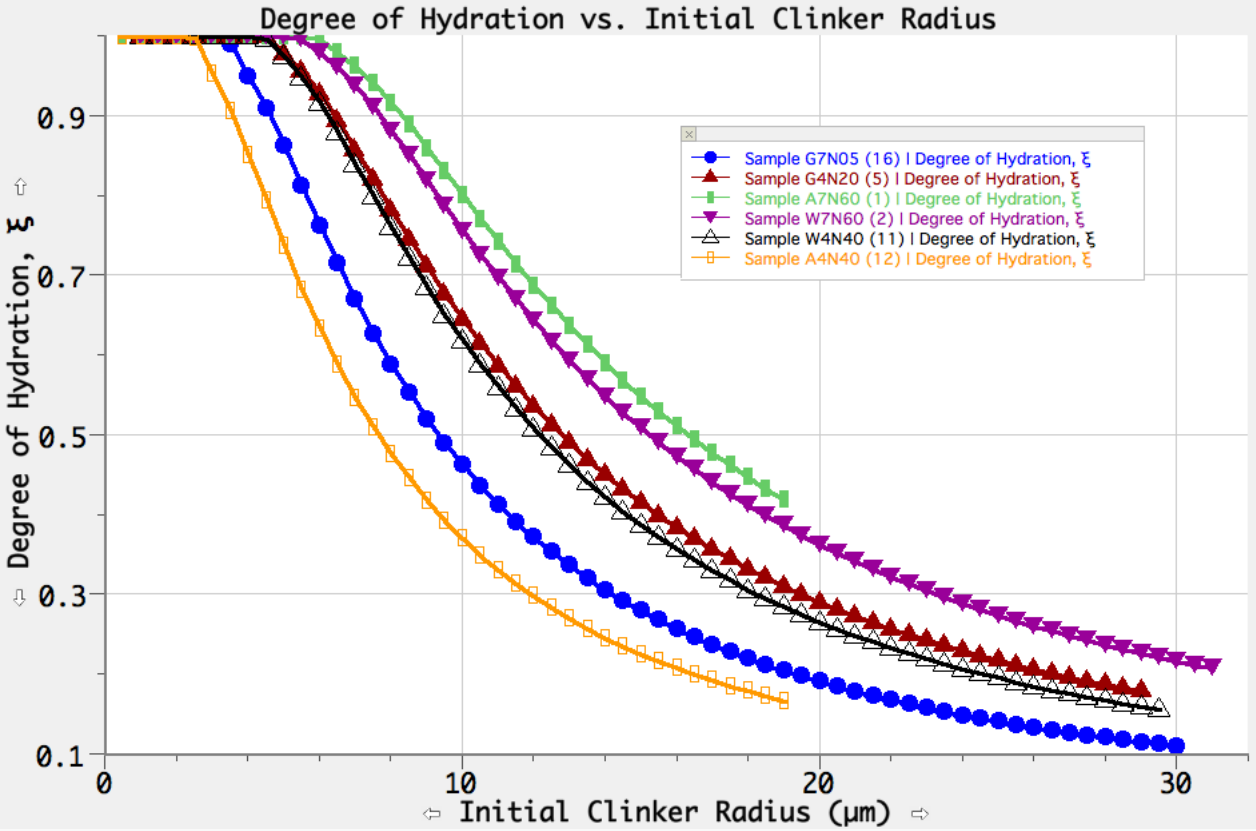

Figure 6-1: Plot of HYMOSTRUC simulated particle hydration at $t = 28days$ as a function of particle radius for samples 1, 2, 5, 11, 12, and 16. A value of 1 represents complete hydration of a particle.

6.2.1 Data Processing

The end goal of using HYMOSTRUC and the Deng-Van Vliet model is to get a relation between hydration and micromechanical strength. In order to do this, the output data from HYMOSTRUC must be linked mathematically to the input data

of the micromechanical model, namely:

$$r_{g,i}(t_1), \xi_i(t_1), \phi(t_1) \Longrightarrow K, G \tag{6.2}$$

where r_g signifies the radius of the clinker surrounded by C-S-H gel at some time t_1, i denotes a size index pertaining to the particle distribution, ξ_i is the size-specific hydration, ϕ is the porosity, and K, G represent the bulk and shear modulus of the composite paste, respectively.

The initial conditions and hydration information can be converted from the distribution information. First, by taking the initial clinker radius $r_{i,c}(t = 0)$ and summing the volume over the number of particles N with size index i, it can be shown that the total initial volume of clinker particles is given as

$$V_{c,0} = \sum_{i=1}^{n} \frac{4\pi}{3} \left(r_{c,i}(0)\right)^3 \cdot N_i. \tag{6.3}$$

The porosity is defined from this as $\phi = V_{c,0}/V_{cell}$. After some time, at $t = t_1$, equation (6.3) can be written as:

$$V_{c,1} = \sum_{i=1}^{n} \frac{4\pi}{3} \left(r_{c,i}(t_1)\right)^3 \cdot N_i. \tag{6.4}$$

At this point, the degree of hydration, ξ, can be defined as:

$$\xi_i = \frac{(r_{c,i}(0))^3 - (r_{c,i}(t_1))^3}{(r_{c,i}(0))^3} \tag{6.5}$$

Due to the coding of the program, each individual particle is allowed to hydrate through adjacent particles such that volume is not conserved upon running the simulation. To counteract this, a correction factor C has been defined as

$$C = \frac{V_{cell}(1 - \phi)}{V_{c,1}}. \tag{6.6}$$

Coupling equation (6.5) and (6.6) yields a corrected total particle plus C-S-H gel

radius (denoted with a star), of

$$r^*_{g,i}(t_1) = \sqrt[3]{\frac{3V_{c,1}}{4\pi N_i C}}. \tag{6.7}$$

In order to obtain the thickness t_g of the entire C-S-H gel (including both HD and LD C-S-H), it is clear that

$$t_g = r^*_{g,i} - r_{c,i}. \tag{6.8}$$

By combining the framework of the hydration model with the Jennings' model, the mass ratio of LD C-S-H to total C-S-H for each size of particle can be calculated using the w/c and hydration values with the relation

$$\frac{m_{LD}}{m_g} = 3.017\frac{w}{c}\xi_i - 1.347\xi_i + 0.538 \tag{6.9}$$

The volume of LD and HD C-S-H is therefore given by

$$V_g = \frac{4\pi}{3}(r^{*3}_{g,i} - r^3_{c,i}), \tag{6.10}$$

$$V_{LD} = V_g \left(\frac{\frac{m_{LD}}{0.63}}{\frac{m_{LD}}{0.63} + \frac{m_{HD}}{0.76}} \right), \tag{6.11}$$

$$V_{HD} = V_g - V_{LD}. \tag{6.12}$$

Now, the outside radius of HD C-S-H surrounding the clinker particle can be determined and used for the micromechanical model developed in Chapter 3:

$$r_{h,i} = \sqrt[3]{\frac{3}{4\pi}V_{HD} + r^3_{c,i}} \tag{6.13}$$

$$K_{EP,i} = K_h \left(1 + \frac{(K_h/K_c - 1)\left(\frac{r_{c,i}(t_1)}{r_{h,i}(t_1)}\right)^3}{1 + \eta_I\left(1 - \left(\frac{r_{c,i}(t_1)}{r_{h,i}(t_1)}\right)^3\right)(1-2\nu_h)(K_h/K_c - 1)} \right)^{-1} \tag{6.14}$$

For the mechanical properties of the entire matrix, we can take the modulus of an

"average particle" by using the Hookean approximation,

$$K_{EP} = \frac{1}{N} \sum_{i=1}^{n} K_{EP,i} \cdot N_i, \tag{6.15}$$

where N is the total number of clinker particles in the system. To find the final mechanical strength of the composite, the relation is thus

$$K = \phi \cdot K_l \left(1 + \frac{(K_l/K_{EP} - 1) f_{EP}}{1 + \eta_I (1 - f_{EP})(1 - 2\nu_l)(K_l/K_{EP} - 1)} \right)^{-1}. \tag{6.16}$$

where f_{EP} represents the ratio of particles to total solid volume (without porosity). For the following results, the following mechanical properties are used:

$$\nu = 0.25, K = \frac{1 - \nu^2}{3(1 - 2\nu)} M = 0.625M \tag{6.17}$$

The results of simulation are displayed in Table 6.3.

Table 6.3: Model results for the hydration of the experimental samples.

Sample No.	K_{EP} (GPa)	f_{EP}	K_{tot} (GPa)	M_{tot} (GPa)
1	21.8	0.48	13.8	**22.0**
2	23.3	0.67	16.5	**26.4**
5	26.7	0.53	15.2	**24.3**
11	25.5	0.67	18.2	**29.2**
12	27.0	0.73	20.7	**32.8**
16	27.8	0.75	21.8	**34.8**

Chapter 7

Instrumented Indentation Results

7.1 Microindentation

Microindentation data were taken for 5 of the 6 samples and analyzed using CSM Instruments Indentation 4.28 software. Using the Oliver-Pharr method, the individual curves were analyzed. An example curve with an optical image of the associated indent is shown in Figure 7-1. The mechanical results from the microindentation tests are presented in Table 7.1.

Table 7.1: Microscale Indentation Modulus Results for the experimental samples. The error reported is the standard mean error.

Sample No.	M (GPa)
1	28.4 ± 0.8
2	–
5	29.0 ± 3.7
11	26.2 ± 1.5
12	34.9 ± 0.54
16	36.1 ± 4.9

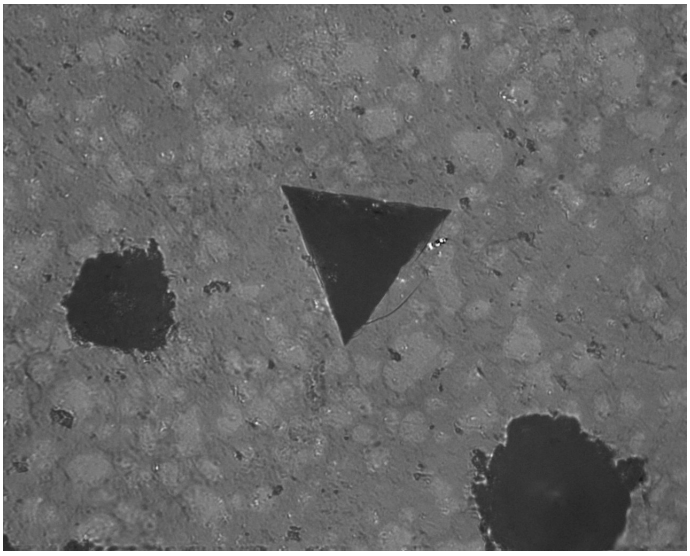

(a)

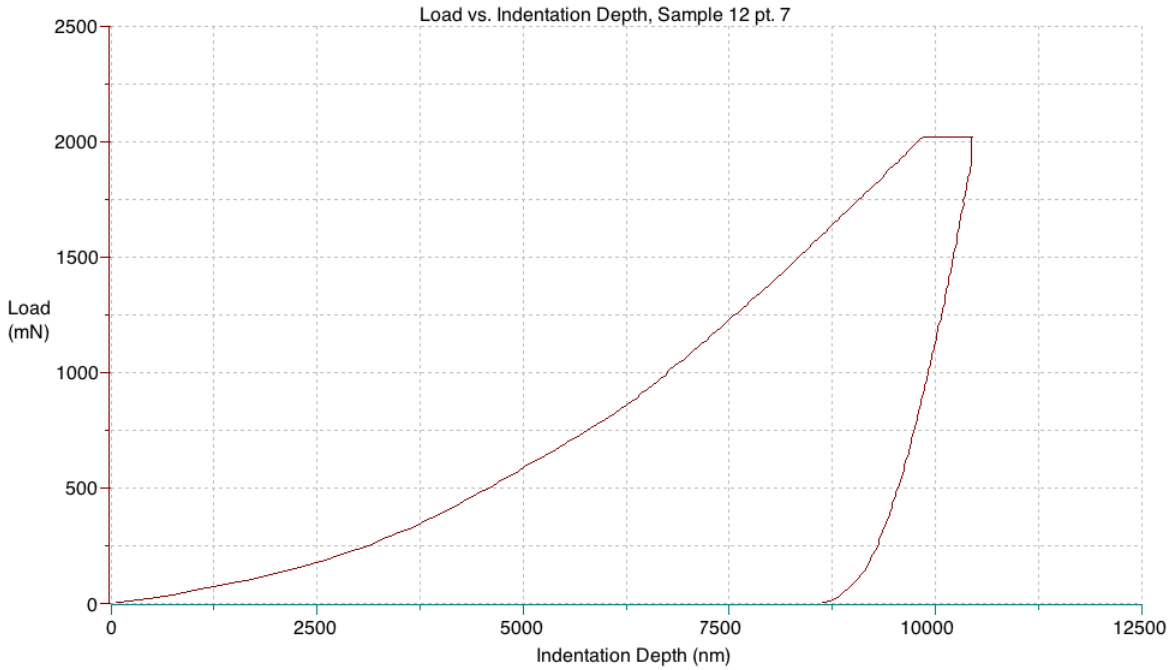

(b)

Figure 7-1: (a) Optical Microscope picture of a microindent on sample 12. (b) The associated load-displacement curve for the same indent trial.

7.2 Nanoindentation

Nanoindentation data were taken for all 6 of the samples and analyzed using the NanoTest platform. Corrections for blunting of the Berkovich tip were taken into account during analysis using the tip-specific Berkovich area function. One thousand (1000) points with associated M and H values (again calculated by the Oliver-Pharr method) were taken per sample, with 800 of those points set in two 400x400 μm grids. Two grids are shown in Figure 7-2. From quick visual inspection, it can be noted that the maps do not match phases point for point, and thus M vs. H is subsequently plotted as well. Individual indentation curves with irregularities in slope were not used in the plots of M vs. H or subsequent analysis, as described in [2]. The plots of M vs. H for all samples are shown in Figure 7-3.

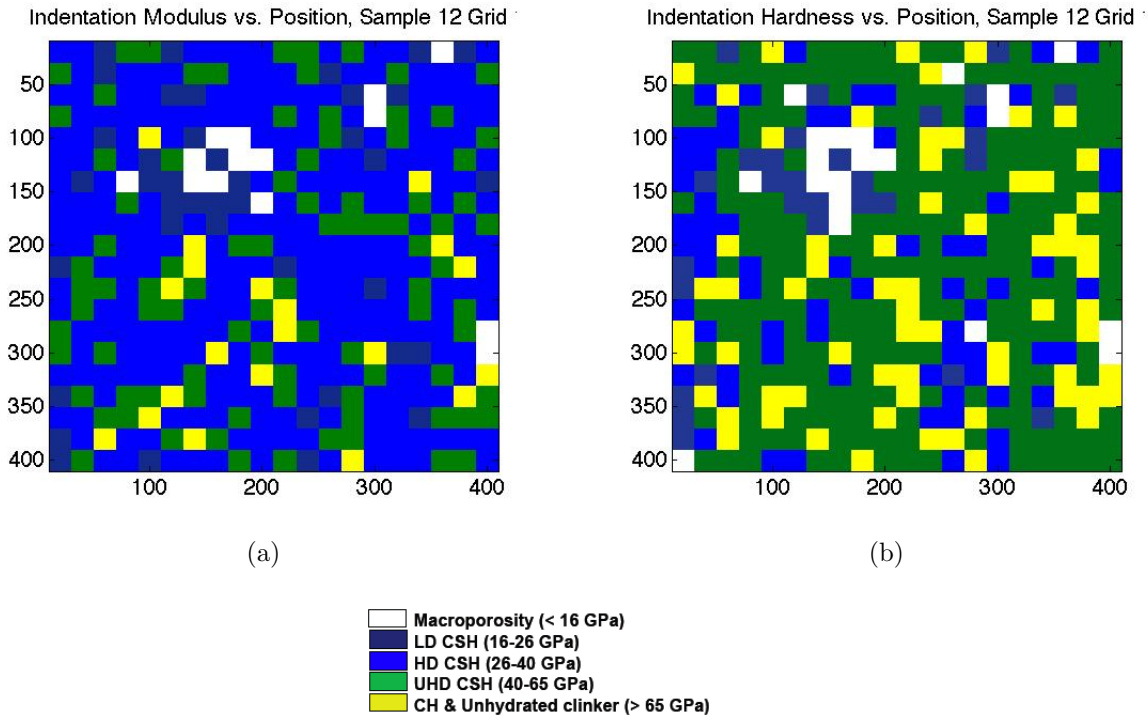

Figure 7-2: Nanoindentation maps of (a) Modulus and (b) Hardness vs. x and y position. Each "voxel" represents an indent at a phase to which the range of hardness or modulus that is typically specific.

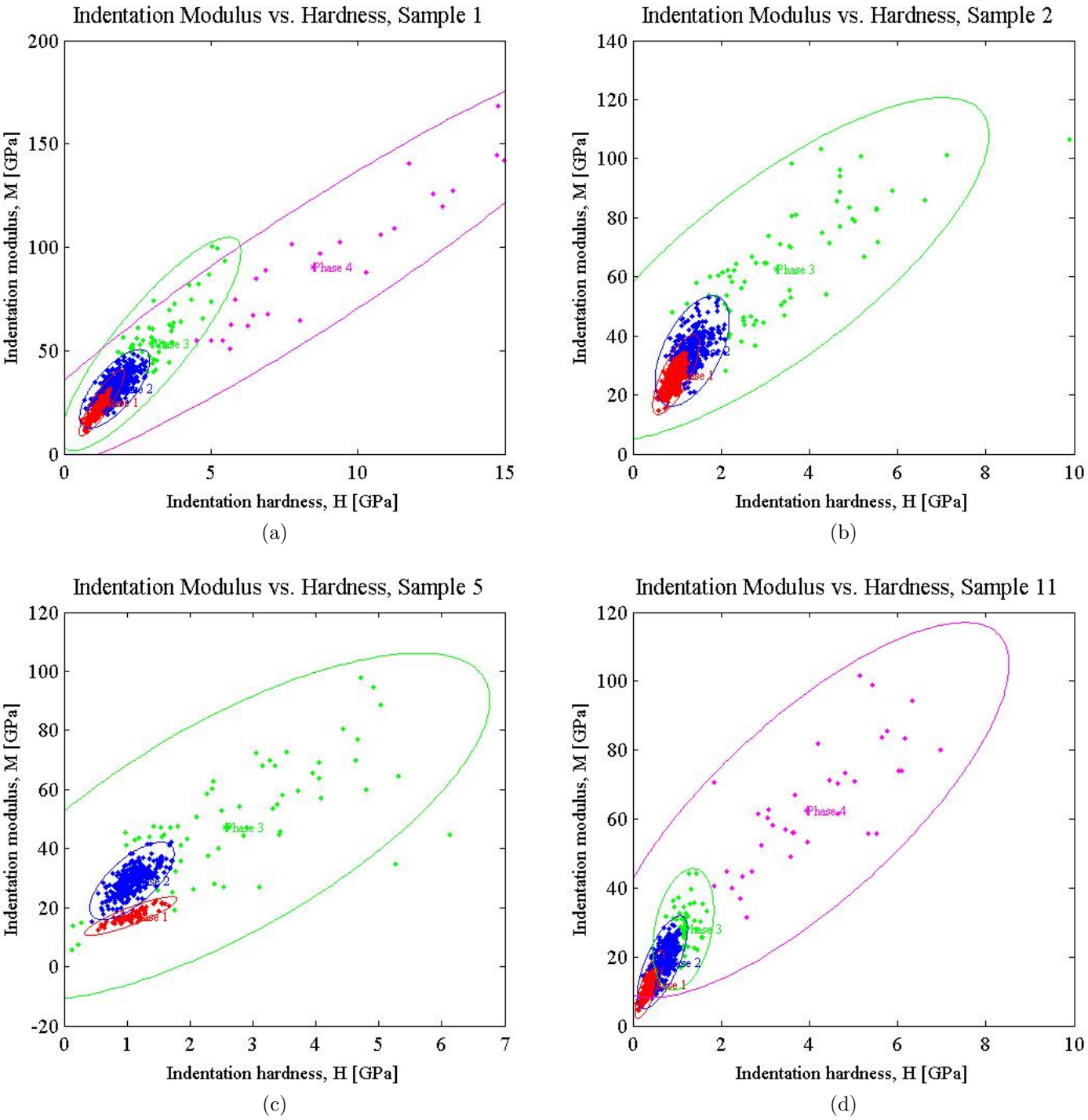

Figure 7-3: The first four graphs of a continued figure. Plots of Indentation Modulus vs. Hardness for Samples 1, 2, 5, and 11 from nanoindentation testing.

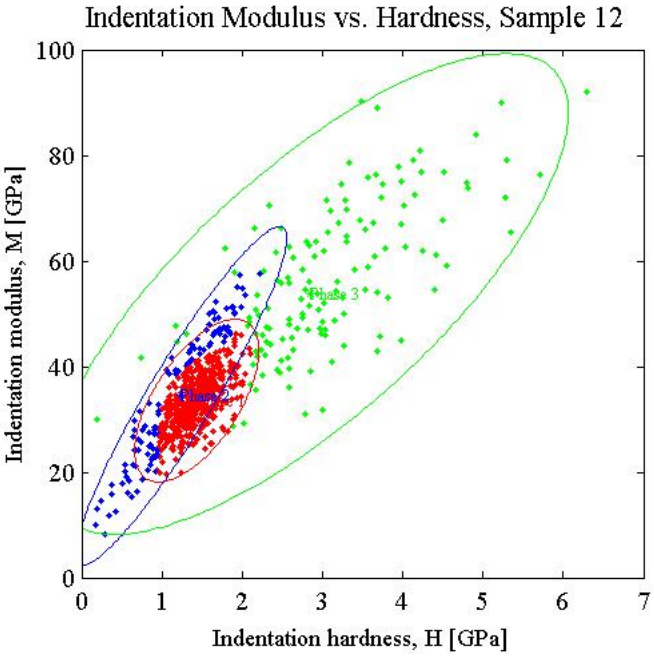

(e)

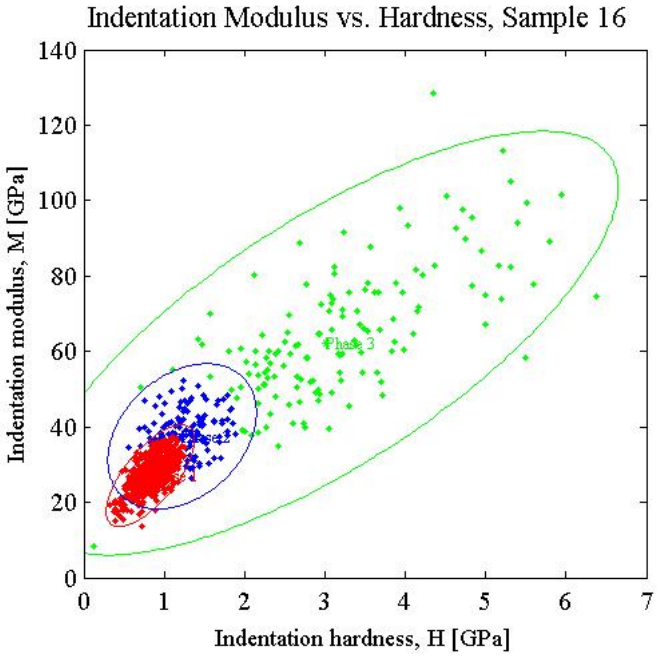

(f)

Figure 7-3: The last two graphs from a continued figure. Plots of Indentation Modulus vs. Hardness for Samples 12 and 16 from nanoindentation testing. The ellipses shown represent clustering results - each ellipse represents a distinct mechanical phase determined by Bayesian statistics.

Part IV

Analysis and Discussion of Results

Chapter 8

Discussion

8.1 Analysis of Results

The first comparison to determine whether the micromechanical hydration model had a physical correlation to the mechanical results is to simply check the resultant moduli of the two systems. However, it is first necessary to identify the relevant sources of error for the hydration model. The factor with the greatest effect on the model is without question, the choice of values for K_l, K_h, and K_c the bulk moduli of the LD C-S-H, HD C-S-H, and clinker phases, respectively. Using Jennings' measured data (see Table 2.2), it can be seen that the indentation modulus of LD C-S-H varies by up to about 22%, while the HD C-S-H modulus varies by about 14%. This is a considerable range on which to predict. Additionally, the influence of portlandite was neglected in the original statement of the C-S-H model. On the scale of microindentation, it is not to be neglected, and thus was accounted for by assuming a 30% volume fraction contribution, as suggested by the chemical model in HYMOSTRUC. The resulting values for the indentation modulus calculated by the micromechanics model plotted with the actual microindentation data is displayed in Figure 8-1.

The first promising result is that the micromechanical calculations are, for the most part, within the experimental range of the microindentation results. Though the sample size is limited (for samples 11 and 16 only two data points were of good enough quality to discern a modulus), the respective moduli are fairly close and mostly within

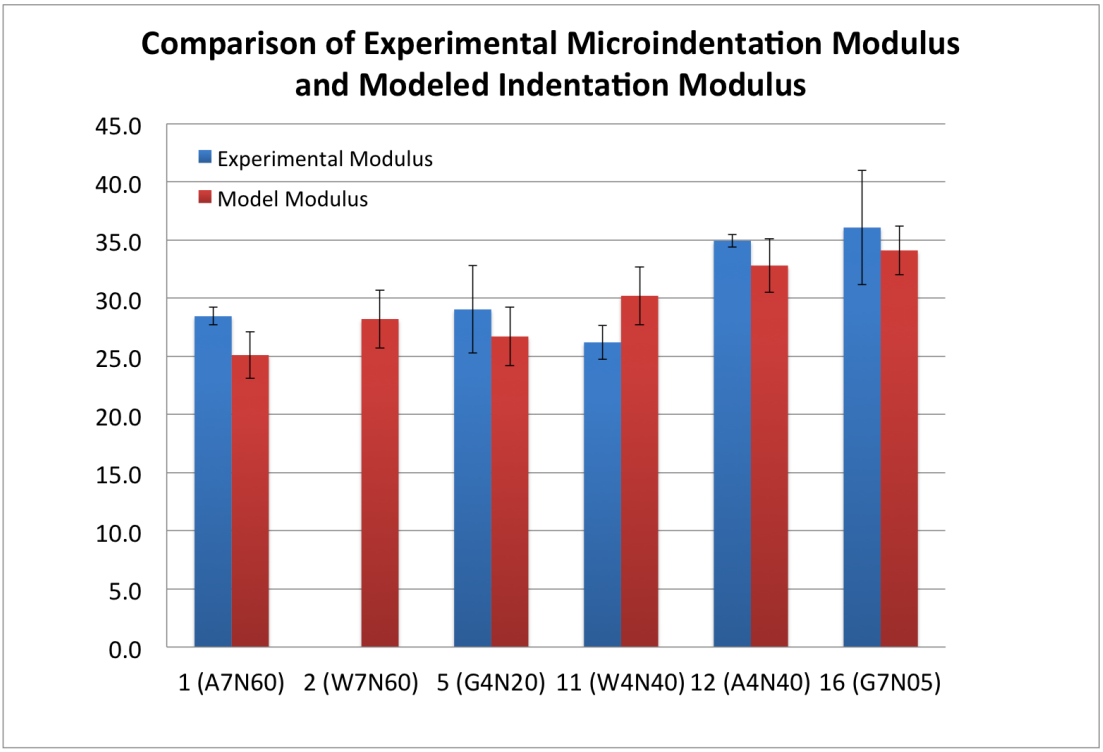

Figure 8-1: Comparison of the experimental microindentation modulus with the developed micromechanical model indentation modulus.

the error range. One reason that two of the samples, 1 and 12, do not have matching values for experimental and modeled modulus is possibly due to the HYMOSTRUC treatment of pure C_3S paste. Referring back to Figure 6-1, samples 12 and 16 have the same w/c ratio, differing clinkers, and slightly different degrees of hydration at time $t = 28d$. However, the pure C_3S is shown to have a lower degree of hydration for most radii. As C_3S is typically responsible for the early strength properties of cement and hydrates quickly, it is counter-intuitive for it to hydrate more slowly than OPC clinker. It is possible, however, as the water amount was constant, that more smaller particles reacted with the water than in the higher-Blaine number white cement or OPC.

Another possible explanation for the microindentation results running slightly high could be a blunted Berkovich indenter probe. Since the machine measures load as a function of displacement while knowing the area also as a function of displacement, any changes to the area would result in misleading numbers. Blunting of the tip would

cause the indenter to register a lower area than what it actually would experience during an indentation. A higher area would lead to a higher applied stress, which would cause the modulus to appear higher than it actually is. Without correcting for the tip area function (which is done for the nanoindentation results but not for microindentation), there is a risk of having overly high modulus values.

Indenter tip blunting is not the sole factor that could alter empirical measurements. Assuming the polishing process has worked reasonably well , which has in fact been analyzed in [11], the sample could still have large residual unhydrated clinker regions. This is largely supported by the fact that various points measured in microindentation were artifacts of indentation on clinker (yielding indentation moduli of about 120 GPa). Clinker aggregates on the scale of microindentation are not accounted for in the micromechanical model - only particles 70 μm and below could be simulated in hydration. Larger particles would likely contribute a higher modulus to the system, which is supported in part by the experimental moduli being mostly higher than the simulated moduli. This could be verified by testing cement pastes with w/c ratios of greater than 0.6, the cutoff for full hydration.

8.2 Connection to Nanoindentation Results

Though the connection between the micromechanical model and microindentation results is an important metric for the success of the hydration model, a more fundamental question remains - *does the system reflect the mechanical variations in C-S-H that are predicted by the various rates of hydration?* The answer can only be determined by probing individual phases using nanoindentation. If the proposed model is correct, there should be not just two disparate phases of C-S-H, but an additional smearing of mechanical properties over the range of HD C-S-H and clinker as described by the effective particle model. Figure 8-2 shows the predicted effective particle mechanical behavior as a function of particle radius for each sample.

As shown in Figure 8-2, each effective particle has its own distinct mechanical properties. Nanoindentation testing should therefore show remnants of this behavior.

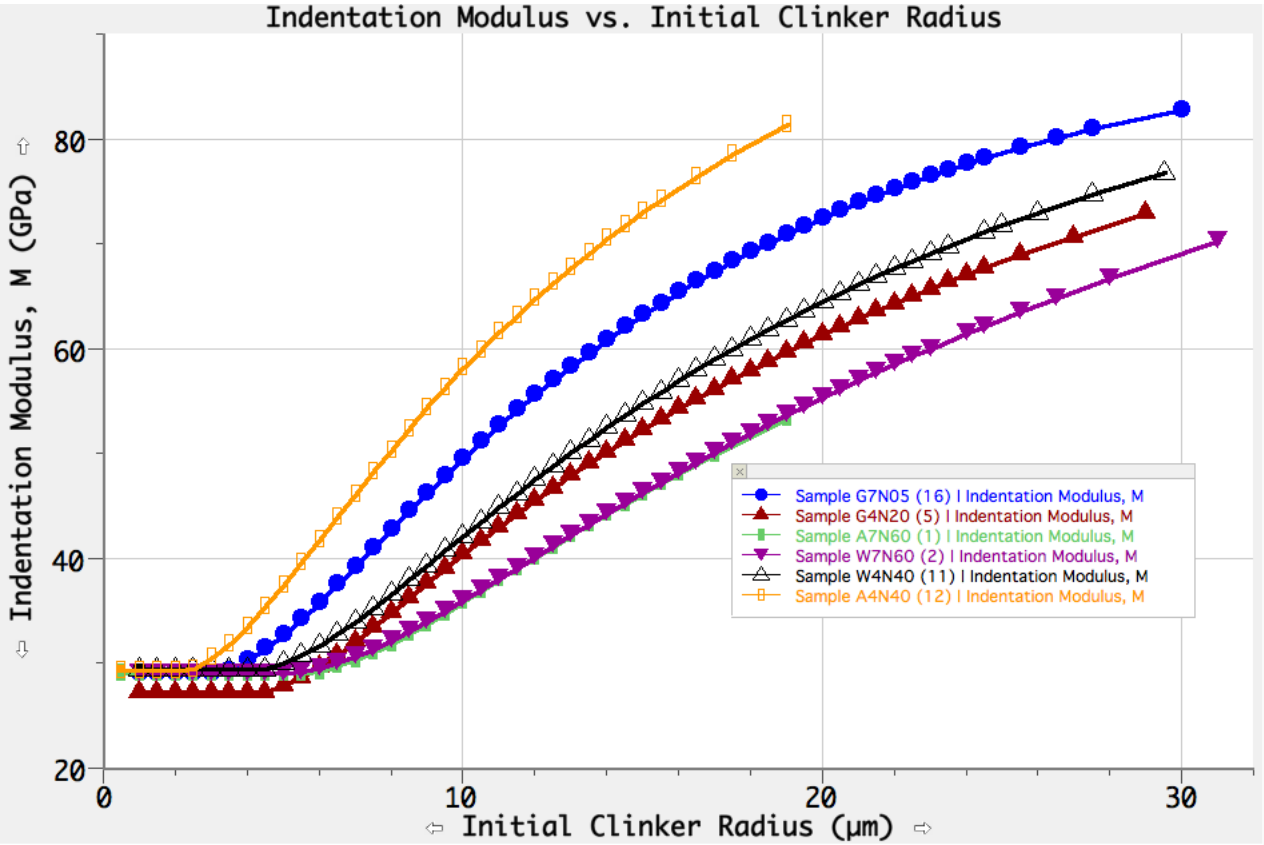

Figure 8-2: Modeled indentation modulus as a function of particle radius for all 6 samples.

Comparison with the results presented in Figure 7-3 show a variation of hardness and modulus values that is not defined by clear LD and HD C-S-H clusters. For this reason, the EMMIX clustering software is used to define, using Bayesian statistics, different characteristic phases of the material. The mean properties of each phase are displayed in Table 8.1. The volume fraction of each phase and corresponding total modulus are then shown in Table 8.2.

The average nanoindentation modulus values are indeed encouraging. By plotting them on the same histogram as the microindentation and model moduli, we can see a fairly good correlation between all three sets of data, as shown in Figure 8-3. This lends support to the validity of the model, as well as suggesting that the mechanical properties from nanoindentation are not simply bimodal, but are in fact a distribution based on the hydration of each individual particle.

It is important to note, that the preparation procedure appears to influence the

Table 8.1: EMMIX clustering results for the nanoindentation moduli of the six samples. Each phase corresponds to the same in Figure 7-3.

Sample No.	M: Phase 1 (GPa)	M: Phase 2 (GPa)	M: Phase 3 (GPa)	M: Phase 4 (GPa)
1	24.8	31.6	53.2	90.2
2	26.9	34.9	62.5	–
5	17.1	29.0	47.3	–
11	12.0	18.5	28.0	62.6
12	33.6	34.4	53.7	–
16	27.1	37.5	62.2	–

Table 8.2: Volume fractions of all respective phases and average modulus of each of the six samples.

Sample No.	f: Phase 1	f: Phase 2	f: Phase 3	f: Phase 4	M_{total}
1	0.39	0.51	0.07	0.03	**32.6±13.0**
2	0.49	0.41	0.10	–	**33.8±10.4**
5	0.14	0.71	0.15	–	**33.0±8.3**
11	0.36	0.49	0.08	0.06	**19.4±11.5**
12	0.57	0.21	0.22	–	**38.1±8.2**
16	0.66	0.15	0.19	–	**35.2±13.5**

final properties of cement in both the hydration model and experimental setup. A decrease in water-to-cement ratio produces a slight increase in indentation modulus, and thus, elastic modulus. For other variations, it is unclear what precise effect each has by itself, due to the nature of the Taguchi setup (i.e. changing all factors without a control for each property). Still harder to discern is the effect of protocol on the samples, but an important modification that should be made is one to reduce porosity in the sample. This severely impacts the nanomechanical testing capabilities for each sample, and could possibly be alleviated by mixing at lower speeds, using a mechanical tamping apparatus, or possibly a vibration table.

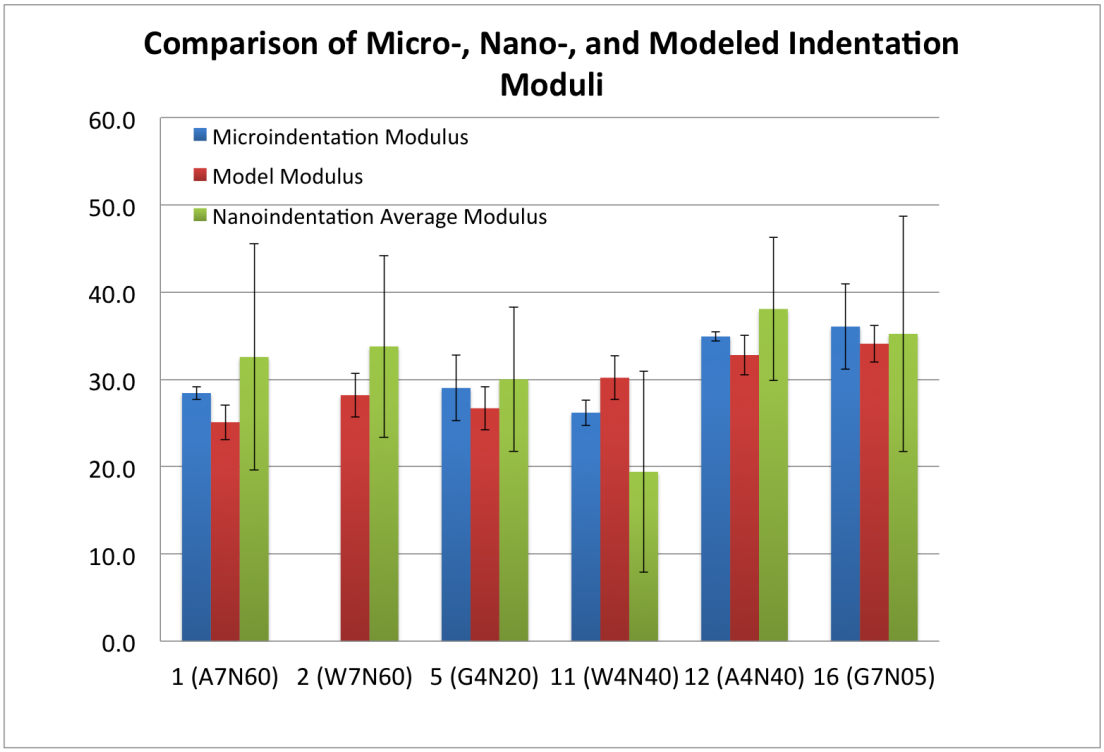

Figure 8-3: Comparison of all three techniques - Nanoindentation, Microindentation, and the Hydration Model Modulus. Note that all are fairly similar in indentation modulus value, giving support to the usability of the developed model.

Chapter 9

Conclusion and Future Investigation

The initial goals of this thesis were fourfold - develop a micromechanical hydration model, develop a synthesis and preparation protocol for cement pastes, implement instrumented indentation testing to determine mechanical properties, and finally correlate the experimental properties with the simulated in order to validate the model. All four goals were in fact, achieved. Using the HYMOSTRUC3D hydration simulation software, a hydration simulation as a function of time and particle distribution was developed. Coupling this with micromechanics theory and a particle with interphase model by Deng and Van Vliet, a mechanical hydration model for cement pastes was developed rigorously. A cement synthesis, curing, and preparation procedure was developed in accordance with both ASTM standards and instrumental requirements, including various additives and clinkers. Both microindentation and nanoindentation were used to mechanically characterize the different cement paste samples on different length scales in order to discern information about how the individual clinker particles influence the entire structure. The micromechanical hydration model's prediction was then compared to actual empirical data and was shown to be within experimental error ranges. The model is currently applicable to cement pastes without aggregate additives such as fly ash, and does not yet explicitly take into account variations such as pH or variations in chemical kinetics due to additives. However, it can certainly

be used for varying water to cement ratios, clinker types, and curing temperatures.

Future possibilities for work in this area would need to address a few main points. The first, and perhaps most important, is the need for more microindentation data. The conclusions made in this thesis are in large part made on a small sample size, and would therefore have to be strengthened by more testing. Furthermore, continued improvements to protocol (such as automation of polishing, etc.) would be welcomed and improve throughput considerably. In terms of a software basis, the most scientifically up-to-date software packages for hydration simulation are that by NIST and the μic software, and would likely present the most informative models going forward.

Taken as a whole, these correlations are a valuable insight to how the hydration of cement behaves. It is only through complete understanding and modeling that we can hope to engineer cement in better and better ways, and this is one humble step towards achieving that goal.

Bibliography

[1] S. Bishnoi and K.L. Scrivener. μic: a new platform for modelling the hydration of cements. *Cement and Concrete Research*, 39:266–274, 2009.

[2] G. Constantinidis. *Invariant Mechanical Properties of Calcium-Silicate-Hydrates (C-S-H) in Cement-Based Materials: Instrumented Nanoindentation and Micro-poromechanical Modeling*. PhD dissertation, Massachusetts Institute of Technology, Department of Civil and Environmental Engineering, February 2006.

[3] F. Deng and K.J. Van Vliet. Prediction of elastic properties for polymer-particle nanocomposites exhibiting and interphase. *Nanotechnology*, 22(165703):7pp, March 2011.

[4] J.D. Eshelby. The elastic field outside and ellipsoidal inclusion. *Proceedings of the Royal Society of London. Series A, Mathematical and Physical Sciences*, 38(1271):561–569, 1959.

[5] Mehta P. K. and Monteiro P. J. M. *Concrete: microstructure, properties and materials.* 2006.

[6] S.H. Kosmatka and W.C. Panarese. *Design and Control of Concrete Mixtures*. Portland Cement Association. Skokie, Illinois, thirteenth edition, .

[7] H.N. Lechtman and L.W. Hobbs. *Seminumerical Algorithms*, volume 3 of *High Technology Ceramics: Past, Present, Future*. American Ceramics Society, 1986. edited by W.D. Kingery.

[8] Jennings H. M. A model for the microstructure of calcium silicate hydrate in cement paste. *Cement and Concrete Research*, 30(1):101–116, 2000.

[9] Jennings H. M. and Johnson S.K. Simulation of microstructure development during the hydration of a cement compound. *J. Am. Ceram. Soc.*, 69:790–795, 1986.

[10] M. Martin and M. Troyon. Fundamental relations used in nanoindentation: Critical examination based on experimental measurements. *J. Mater. Res.*, 17(9), September 2002.

[11] Bobko C. Vandamme M. Miller, M. and F.-J. Ulm. Surface roughness criteria for cement paste nanoindentation. *Cement and Concrete Research*, 38:467–476, 2008.

[12] W.C. Oliver and G.M. Pharr. Measurement of hardness and elastic modulus by instrumented indentation: Advances in understanding and refinements to methodology. *J. Mater. Res.*, 7(1564), 1992.

[13] William J. Parnell. A brief history of homogenization and micromechanics, with applications. Lecture, School of Machematics, Universite Paris, April 2010.

[14] Tennis P.D. and Jennings H. M. A model for two types of calcium silicate hydrate in the microstructure of portland cement pastes. *Cement and Concrete Research*, 30(6):855–863, 2000.

[15] E. Sanchez-Palencia. Homogenization techniques for composite media. Lectures Delivered at the CISM International Center for Mechanical Sciences Udine, Italy, July 1985.

[16] Shahsavari R. et al. Stewart, K. Designing liquid stone: Modulating cement mechanics via computational and physical chemistry. Awaiting Publishing, 2011.

[17] United States Geological Survey. Cement. Mineral Commodity Summaries, January 2011.

[18] H.F.W. Taylor. *Cement Chemistry*. Thomas Telford Publishing, 1 Heron Quay, London, U.K., second edition, Copyright 1997.

[19] Biernacki J.J. Bullard et al. Thomas, J.J. Modeling and simulation of cement hydration kinetics and microstructure development. *Cement and Concrete Research*. Corrected Proof, Available online 2 February 2011.

[20] M. Vandamme. *The Nanogranular Origin of Concrete Creep: A Nanoindentation Investigation of Microstructure and Fundamental Properties of Calcium-Silicate-Hydrates*. PhD dissertation, Massachusetts Institute of Technology, Department of Civil and Environmental Engineering, June 2008.